



ELSEVIER

Available online at [www.sciencedirect.com](http://www.sciencedirect.com)

SCIENCE @ DIRECT®

NDT&E International 36 (2003) 339–348

**NDT&E**  
international

[www.elsevier.com/locate/ndteint](http://www.elsevier.com/locate/ndteint)

## On the role of material property gradients in noncontacting thermoelectric NDE

Hector Carreon, Balachander Lakshminarayan, Waseem I. Faidi,  
Adnan H. Nayfeh, Peter B. Nagy\*

*Department of Aerospace Engineering and Engineering Mechanics, University of Cincinnati, Cincinnati, OH 45221-0070, USA*

Received 5 December 2001; revised 10 December 2002; accepted 20 December 2002

### Abstract

Inclusions and other types of imperfections in nonmagnetic metals can be nondestructively detected by noncontacting magnetic measurements that sense the thermoelectric currents produced by directional heating and cooling of the specimen. The detectability of small and/or weak imperfections is ultimately limited by the intrinsic anisotropy and inhomogeneity of the material to be inspected. This paper investigates the spurious magnetic signature produced by the simplest type of macroscopic inhomogeneity when the material properties exhibit a linear spatial variation in the cross section of a slender bar. An analytical method has been developed for calculating the normal and tangential magnetic fields produced by the resulting thermoelectric currents. Experimental results from a highly inhomogeneous artificial copper/brass sintered specimen were found to be in very good quantitative agreement with our theoretical predictions and fully verified our analytical model. Similar measurements on a weakly inhomogeneous Ti–6Al–4V titanium-alloy bar were also shown to be in very good qualitative agreement with the predictions of the analytical model although the unexpectedly high magnitude of the observed signatures could not be verified by conventional contact measurements, therefore further efforts are needed to better understand the underlying physical phenomenon and clarifying the relationship between the strength of the signature and the very complex microstructural features of this popular high-strength alloy.

© 2003 Elsevier Science Ltd. All rights reserved.

*Keywords:* Thermoelectric NDE; Magnetic detection; Inhomogeneity

### 1. Introduction

Conventional thermoelectric techniques are uniquely sensitive to intrinsic material variations, but are basically insensitive to external geometrical effects such as the size, shape, and surface quality of the specimen to be tested. Essentially all existing thermoelectric NDT techniques are based on the well-known Seebeck effect that is commonly used in thermocouples to measure temperature at the junction of two different conductors. Ideally, regardless of the temperature difference between the junctions, only thermocouples made of different materials, or more precisely, materials of different thermoelectric power, will generate a thermoelectric signal. This unique feature makes the simple thermoelectric tester one of the most sensitive material discriminators used in nondestructive inspection.

The thermoelectric power of metals is sensitive to variety of material properties that can affect the measurement. Clearly, chemical composition exerts the strongest effect on the thermoelectric properties and accordingly the basic application of thermoelectric materials characterization is metal sorting [1]. However, it is well known that under special conditions, materials of identical chemical composition can also produce an efficient thermocouple as a result of different heat treatment, hardening, texture, residual stress, fatigue, etc., which can be further exploited for nondestructive testing of materials [2–5].

Sensitive thermoelectric detection requires that a reference electrode of very similar material be used so that the adverse effects of inevitable temperature uncertainties could be minimized. In addition, very good metallic contact must be established between the reference electrodes and the part to be inspected. The application of the conventional thermoelectric technique in nondestructive materials characterization is badly limited by the spurious effects of

\* Corresponding author. Tel.: +1-513-556-3353; fax: +1-513-556-5038.  
E-mail address: [peter.nagy@uc.edu](mailto:peter.nagy@uc.edu) (P.B. Nagy).

the imperfect contact interface between the hot electrode and the specimen [4]. The resulting thermoelectric offset can be reduced, but not entirely eliminated, by decreasing the thermal and electrical resistance between the specimen and the reference electrode (e.g. via better cleaning or imposing higher contact pressure). Ultimately, the presence of this imperfect contact limits the detectability of small variations in material properties by the conventional thermoelectric technique. When either small inclusions or subtle local variations such as texture, hardening, fatigue damage, or weak impurities are to be detected, the best sensitivity can be achieved by using the surrounding intact material as the reference electrode. This so-called self-referencing method not only provides an ideal reference electrode, but also automatically eliminates the above mentioned spurious thermoelectric offset caused by having a less than perfect interface between the part to be tested and the surrounding intact reference material.

It was first suggested by Hinken and Tavrín [6] and more recently by Maslov and Kinra [7] that self-referencing thermoelectric measurements can also be done in an entirely noncontacting way by using high-sensitivity magnetic detectors to sense the weak thermoelectric currents around inclusions and other types of inhomogeneities when the specimen to be tested is subjected to directional heating or cooling. A schematic diagram of the self-referencing thermoelectric method with noncontacting magnetic sensing is shown in Fig. 1. External heating or cooling is applied to the specimen to produce a modest temperature gradient ( $\approx 1$  °C/cm) in the region to be tested. As a result, different points of the boundary between the host material and the inclusion will be at different temperatures, therefore also at different thermoelectric potentials. These potential differences will produce opposite thermoelectric currents inside and outside the inclusion. The thermoelectric currents form two local loops that run in opposite directions on the two sides of the inclusion relative to the prevailing heat flux,

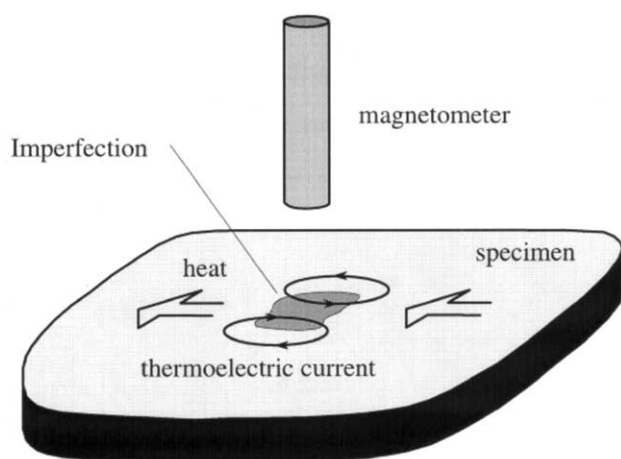


Fig. 1. A schematic diagram of noncontacting detection of material imperfections by magnetic monitoring of thermoelectric currents.

which can be detected by scanning the specimen with a sensitive magnetometer. Since the surrounding intact material serves as the 'reference' electrode and there is no artificial interface between the host and the imperfect region to be detected, the detection sensitivity to variations in material properties could be very high assuming that the absolute sensitivity of the magnetometer is sufficient to pick up the weak external magnetic field produced by the thermoelectric currents inside the specimen.

It was recently demonstrated that the noncontacting thermoelectric technique can be used to detect various imperfections in conducting metals, including foreign body inclusions and more subtle local property variations caused by service or manufacturing related effects such as cold work, localized texture, residual stress, excess heat, fatigue damage, fretting, etc. [6–14]. Like most other methods used in NDE, the detection sensitivity of the noncontacting thermoelectric method is ultimately limited by temporally coherent material noise rather than temporally incoherent electrical noise, which could be easily eliminated by simple time averaging. Strictly speaking, material 'noise' is really unwanted background 'signal' that is often called noise only because it interferes with, and often conceals, the flaw signals to be detected. The main sources of such adverse background signals in thermoelectric NDE are macrostructural features such as case hardening, cold work, texture induced anisotropy, residual stress, etc., while small-scale microstructural features such as grains are less important because of the lack of sufficient spatial resolution.

The detection probability of small and/or weak imperfections in metals depends on the thermoelectric background signature produced by the intrinsic anisotropy and inhomogeneity of the material [11]. In a recent paper, we studied the effect of anisotropic texture in a homogeneous material and developed an analytical model capable of quantitatively predicting the resulting thermoelectric signature for simple inspection of geometries [12]. In this paper, our goal is to develop and experimentally verify an analytical model capable of predicting the thermoelectric background signature caused by weak material inhomogeneity for the simplest and most common inspection geometry, namely, in the case of an axially heated slender rectangular bar.

Of course, real specimens often exhibit both anisotropy and inhomogeneity, therefore, the measured magnetic signature is due to a combination of both effects. Whether the actual signature is dominated by anisotropy or inhomogeneity of the specimen can be established on a case-to-case basis by comparing the signatures recorded after rotating the specimen around its principal (length, width, and thickness) axes. Since anisotropic properties are invariant for 180° rotations, the true source of the magnetic signature can always be established by repeated measurements at different orientations of the bar. This technique will be discussed in more detail in the experimental part of this paper. At this point, it is sufficient to say that in many cases

we found that the shape of the background signature essentially remained the same but flipped its sign when the specimen was rotated by 180° around the direction of heat propagation, which clearly indicates that the observed signal cannot originate from the anisotropy of the specimen unless it is also inhomogeneous [12]. We will also show that this rotational symmetry can be exploited not only to separate anisotropic effects from those of inhomogeneity, but also to further separate the two principal inhomogeneity components in the thickness and width-directions from each other.

## 2. Analytical model

In this section, we are going to present a simple analytical model to predict the magnetic background signature caused by linear inhomogeneity in an isotropic medium. Thermoelectricity is a result of intrinsically coupled transport of electricity and heat, that can be expressed by the following constitutive relationship [15]

$$\begin{bmatrix} \mathbf{j} \\ \mathbf{h} \end{bmatrix} = \begin{bmatrix} \sigma & \sigma S \\ \sigma S T & \kappa \end{bmatrix} \begin{bmatrix} -\nabla\Phi \\ -\nabla T \end{bmatrix}, \quad (1)$$

where  $\mathbf{j}$  is the electrical current density,  $\mathbf{h}$  is the thermal flux,  $\Phi$  is the electric potential,  $T$  is the temperature,  $\sigma$  denotes the electrical conductivity measured at uniform temperature,  $\kappa$  is the thermal conductivity for zero electrical field, and  $S$  is the absolute thermoelectric power of the material. Assuming weak thermoelectric coupling, steady-state solutions can be obtained by requiring that  $\nabla \cdot \mathbf{h} = 0$  [10]. In addition, Maxwell’s law requires that  $\nabla \cdot \mathbf{j} = 0$ . The determinant of the matrix in Eq. (1) is  $\sigma(\kappa - \sigma S^2 T) = \sigma k$ , where  $k$  is the thermal conductivity for zero electrical current. Noting that  $\sigma k \neq 0$ ,  $\nabla \cdot \mathbf{h} = 0$  and  $\nabla \cdot \mathbf{j} = 0$  require that the Laplacians of  $T$  and  $\Phi$  vanish individually, i.e.

$$\nabla^2 T = 0 \text{ and } \nabla^2 \Phi = 0. \quad (2)$$

For a homogeneous isotropic medium,  $\sigma$ ,  $\kappa$ , and  $S$  are scalar quantities that do not depend directly on the spatial coordinates, though generally they do depend on temperature, which can introduce an indirect spatial variation. For purely thermal excitation in an isotropic medium, the local electrical field  $\mathbf{E} = -\nabla\Phi$  is strictly parallel to the temperature gradient  $\nabla T$  and the electrical current density

can be shown to identically vanish everywhere. This means that, regardless of the size, shape, and material properties of a homogeneous isotropic specimen, no thermoelectric current will be generated by any type of heating or cooling. However, in the presence of material inhomogeneity, the thermoelectric current does not necessarily vanish in the specimen, a condition that can be easily detected by external noncontacting magnetic sensors.

Let us consider a slender bar of rectangular cross section with length  $\ell$  much larger than its two other dimensions. The bar is aligned with the  $z$ -direction of a Cartesian coordinate system  $(x, y, z)$  as shown in Fig. 2. In the simplest first-order approximation of inhomogeneity, the spatial dependence of the material properties can be assumed to follow linear profiles

$$\kappa \approx \kappa_0(1 + a_x x + a_y y + a_z z + \dots), \quad (3a)$$

$$\sigma \approx \sigma_0(1 + b_x x + b_y y + b_z z + \dots), \quad (3b)$$

$$S \approx S_0(1 + c_x x + c_y y + c_z z + \dots). \quad (3c)$$

Here, the subscripts 0 refer to the average values of the material properties, while  $a$ ,  $b$  and  $c$  are property gradients characterizing the material inhomogeneity. In the case under consideration, material variations along the length of the bar can be neglected partly because the technological effects responsible for the development of linear inhomogeneity (e.g. cold work, residual stress, etc.) do not cause significant axial variations in the material properties and partly because only material variations normal to the direction of heat propagation cause thermoelectric currents. In order to further simplify our analytical model, we are going to assume property variations along the  $y$ -direction only

$$\kappa = \kappa_0(1 + ay), \quad \sigma = \sigma_0(1 + by), \quad S = S_0(1 + cy), \quad (4)$$

where we dropped the  $y$  subscript for brevity. Later, we will present experimental evidence that lateral variations in both thickness and width-directions of the bar contribute to the observed magnetic signatures. However, this more general two-dimensional inhomogeneity can be easily handled by the one-dimensional model using superposition.

The bar is subjected to a uniform axial heat flux  $h_0$  along the  $z$ -axis while its sides at  $x = \pm w/2$  and  $y = \pm t/2$  are assumed to be insulated, i.e. we assume that the heat conducted through the metallic bar is much larger than

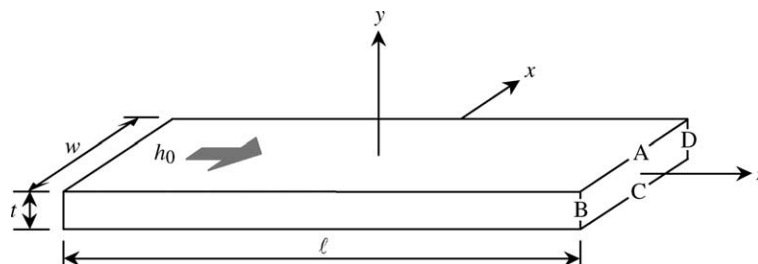


Fig. 2. The geometrical arrangement of the rectangular bar and the Cartesian coordinate system used in the analytical calculations.

the heat lost by convection and radiation to the surrounding environment. These assumptions reduce the thermoelectric problem into a two-dimensional one in the  $y, z$  plane. Imposing the one-dimensional spatial distribution of Eq. (4) on the field equations given by Eq. (2) yields the following coupled governing equations

$$\kappa \left[ \frac{\partial^2 T}{\partial y^2} + \frac{\partial^2 T}{\partial z^2} \right] + \frac{\partial \kappa}{\partial y} \frac{\partial T}{\partial y} = 0, \quad (5)$$

$$\begin{aligned} \sigma S \left[ \frac{\partial^2 T}{\partial y^2} + \frac{\partial^2 T}{\partial z^2} \right] + \sigma \left[ \frac{\partial^2 \Phi}{\partial y^2} + \frac{\partial^2 \Phi}{\partial z^2} \right] \\ + \left[ S \frac{\partial \sigma}{\partial y} + \sigma \frac{\partial S}{\partial y} \right] \frac{\partial T}{\partial y} + \frac{\partial \sigma}{\partial y} \frac{\partial \Phi}{\partial y} \\ = 0, \end{aligned} \quad (6)$$

where we omitted the contribution of the electric field to the heat flux since it is negligible for the typically very low values of the thermoelectric coupling in metals [10]. The exact analytical solution of these coupled equations for arbitrary boundary conditions is fairly complicated. However, for the slender bar under consideration, the complicated temperature and electrical potential distributions near ends are irrelevant far away from the ends, and  $T$  and  $\Phi$  will be simple linear functions of  $z$  only, i.e.  $T = T(z) = Az$  and  $\Phi = \Phi(z) = A^*z$ , where  $A$  and  $A^*$  are currently unknown constants. Since the sides of the bar are assumed to be insulated, the total heat flux across any cross section normal to the  $z$ -axis is conserved and should be equal to the total heat flow  $\dot{Q} = h_0 w t$ , where  $h_0$  denotes the average heat flux density. Now, far away from the ends  $\dot{Q}$  may be estimated as

$$\dot{Q} = -w \frac{dT}{dz} \int_{-t/2}^{t/2} \kappa(y) dy = -t w A \kappa_0, \quad (7)$$

therefore

$$T = -\frac{h_0}{\kappa_0} z = \nabla T z. \quad (8)$$

The net electric current through any normal cross section of the bar should be zero

$$\begin{aligned} \int_{-t/2}^{t/2} j_z(y) dy = -\frac{d\Phi}{dz} \int_{-t/2}^{t/2} \sigma(y) dy - \frac{dT}{dz} \int_{-t/2}^{t/2} \sigma(y) S(y) dy \\ = 0, \end{aligned} \quad (9)$$

which yields

$$\Phi \approx -\nabla T S_0 z, \quad (10)$$

where we exploited that the relative inhomogeneity is low, i.e.  $bct^2 \ll 1$ . Now, we can substitute Eqs. (8) and (10) into the constitutive relations (1) to obtain the electric current density

$$j_z = -\sigma_0 S_0 c \nabla T y = j_0 y, \quad (11)$$

where  $j_0$  is a constant determined by the material properties and  $j_x = j_y = 0$ . In Eq. (11), we exploited again that the relative inhomogeneity is low.

Generally, the magnetic field produced by the thermoelectric currents can be calculated using the Biot–Savart law

$$\mathbf{H}(\mathbf{x}) = \int_{-\ell/2}^{\ell/2} \int_{-t/2}^{t/2} \int_{-w/2}^{w/2} \frac{\mathbf{j}(\mathbf{X}) \times (\mathbf{x} - \mathbf{X})}{4\pi |\mathbf{x} - \mathbf{X}|^3} dXdYdZ, \quad (12)$$

where  $\mathbf{x}$  and  $\mathbf{X}$  are coordinate vectors of the point of observation and the differential volume of the bar, respectively. Far away from the ends of the long bar neither the electric current density nor the associated magnetic field depends on  $z$ , therefore, without loss of generality, we can evaluate the integral at  $z = 0$ . Performing the cross product in Eq. (12) and integrating along the length of the bar yields

$$H_x(x, y) = -\frac{j_0}{2\pi} \int_{-t/2}^{t/2} \int_{-w/2}^{w/2} \frac{Y(y - Y)}{(x - X)^2 + (y - Y)^2} dXdY, \quad (13a)$$

and

$$H_y(x, y) = \frac{j_0}{2\pi} \int_{-t/2}^{t/2} \int_{-w/2}^{w/2} \frac{Y(x - X)}{(x - X)^2 + (y - Y)^2} dXdY. \quad (13b)$$

Integration with respect to  $X$  reduces the integrals to the following one-dimensional forms

$$\begin{aligned} H_x(x, y) = -\frac{j_0}{2\pi} \int_{-t/2}^{t/2} Y \left\{ \tan^{-1} \left[ \frac{x + w/2}{y - Y} \right] \right. \\ \left. - \tan^{-1} \left[ \frac{x - w/2}{y - Y} \right] \right\} dY, \end{aligned} \quad (14a)$$

$$H_y(x, y) = \frac{j_0}{4\pi} \int_{-t/2}^{t/2} Y \ln \left[ \frac{(x + w/2)^2 + (y - Y)^2}{(x - w/2)^2 + (y - Y)^2} \right] dY. \quad (14b)$$

Finally, the integrals in Eqs. (14) can be solved as follows

$$\begin{aligned} H_x(x, y) = H_0 \left[ F_x(x + w/2, y) \Big|_{-t/2}^{t/2} \right. \\ \left. - F_x(x - w/2, y, Y) \Big|_{-t/2}^{t/2} \right], \end{aligned} \quad (15a)$$

$$\begin{aligned} H_y(x, y) = H_0 \left[ F_y(x + w/2, y, Y) \Big|_{-t/2}^{t/2} \right. \\ \left. - F_y(x - w/2, y, Y) \Big|_{-t/2}^{t/2} \right], \end{aligned} \quad (15b)$$

where after some algebraic simplifications

$$\begin{aligned} F_x(\xi, y, Y) = \xi y \ln \left[ 1 + \left( \frac{y - Y}{\xi} \right)^2 \right] + \xi Y + (Y^2 - y^2 + \xi^2) \\ \times \tan^{-1} \left[ \frac{y - Y}{\xi} \right], \end{aligned} \quad (16a)$$

$$F_y(\xi, y, Y) = \frac{Y^2 - y^2 + \xi^2}{2} \ln \left[ 1 + \left( \frac{y - Y}{\xi} \right)^2 \right] - yY - 2\xi y \tan^{-1} \left[ \frac{y - Y}{\xi} \right], \quad (16b)$$

and

$$H_0 = \frac{j_0}{4\pi} = -\frac{1}{4\pi} \sigma_0 S_0 c \nabla T. \quad (16c)$$

### 3. Experimental method

In this section, we will describe the experimental setup and procedure we used to verify that the previously introduced analytical model properly predicts the normal and tangential components of the magnetic field produced by thermoelectric currents induced in an inhomogeneous specimen when it is subjected to an external temperature gradient. A Ti–6Al–4V titanium-alloy specimen of length  $\ell = 203$  mm, width  $w = 12.7$  mm, and thickness  $t = 6.35$  mm was cut from a cold-rolled plate. At an arbitrarily chosen orientation, the top, left, bottom, and right sides of the bar were marked as A, B, C, and D, respectively. Then, any other orientation can be easily identified by the order of the edges progressing in a counter-clockwise direction starting from the top. For example, CBAD, ADCB, and CDAB correspond to  $180^\circ$  rotations around the  $x$ ,  $y$ , and  $z$  axes, respectively.

In order to establish whether the specimen was strongly inhomogeneous and/or anisotropic, we measured the electrical conductivity and absolute thermoelectric power on the four sides of the specimen. First, we used a US-450 (UniWest Corp.) eddy current instrument with a 1.5 mm diameter probe coil at 1 MHz to measure the electrical conductivity. The system was calibrated on reference materials of known electrical conductivity. One hundred readings were taken on each side and then averaged to get a representative value. On sides A (0.587 MS) and C (0.590 MS) the electrical conductivity was found to be significantly higher than on sides B (0.572 MS) and D (0.570 MS). The  $\approx 3\%$  difference between sides A and C versus sides B and D was well above the standard deviation (0.003 MS or 0.5%), which indicates the presence of significant anisotropy in electrical conductivity. On the other hand, the small difference between sides A and C or sides B and D was less than the standard deviation, therefore, we can conclude that conventional eddy current inspection could not unequivocally verify the presence of a significant inhomogeneity in electrical conductivity.

Second, we measured the thermoelectric power with an ATS-6044 Alloy ThermoSorter (Walker Scientific, Inc.) in an attempt to establish the presence of thermoelectric anisotropy and/or inhomogeneity. Again, the equipment

was calibrated on reference materials of known absolute thermoelectric power and 100 readings were taken on each side of the Ti–6Al–4V specimen and then averaged to get a representative value. On sides A ( $-5.09 \mu\text{V}/^\circ\text{C}$ ) and C ( $-5.11 \mu\text{V}/^\circ\text{C}$ ), the thermoelectric power was found to be of significantly higher magnitude than on sides B ( $-4.69 \mu\text{V}/^\circ\text{C}$ ) and D ( $-4.72 \mu\text{V}/^\circ\text{C}$ ). The  $\approx 8\%$  difference between sides A and C versus sides B and D was again above the standard deviation ( $0.15 \mu\text{V}/^\circ\text{C}$  or 3%), which indicates the presence of a significant anisotropy in thermoelectric power. As before, the small difference between sides A and C or sides B and D was less than the standard deviation, therefore we can conclude that conventional thermoelectric inspection could not unequivocally verify the presence of significant thermoelectric inhomogeneity in the specimen.

In spite of the apparently stronger effect of anisotropy, the thermoelectric background signature of a slender bar could be still dominated by the inhomogeneous contribution because the heat flux is forced to be parallel to the axis of the bar. This could be easily verified by rotating the bar by  $180^\circ$ , upon which the signature should not change at all if it were caused by anisotropy. We found that the signature of the specimen was essentially reversed upon such rotation, therefore, it was primarily due to inhomogeneity. We also noticed that the observed change in the signature also depended on how the  $180^\circ$  rotation was executed. The obvious reason for this is that, in contrast with our simple analytical model, the specimen exhibited property gradients in both width and thickness-directions. Fig. 3 shows (a) the true two-dimensional inhomogeneity of the specimen and how addition and subtraction of different profiles can be used to eliminate either the (b) width or (c) thickness-component of the inhomogeneity.

Fig. 4 shows a schematic diagram for the experimental arrangement used to study the different thermoelectric signatures produced by the bar. The fluxgate magnetometer can be polarized either tangentially or normal to the top surface in order to measure the  $x$  and  $y$  components of the magnetic field, respectively. The specimen was mounted on two copper supports that also acted as heat exchangers to facilitate efficient heating and cooling and the whole assembly was mounted on a non-magnetic translation table for scanning. In order to improve the heat transfer, a layer of heat conducting silicone grease compound was applied between the specimen and the copper heat exchangers, which were heated and cooled to temperatures of 85 and 5  $^\circ\text{C}$ , respectively. The actual temperature of the Ti–6Al–4V specimen was monitored by thermocouples at two points and the temperature gradient along the center part of the bar was kept at 4.5  $^\circ\text{C}/\text{cm}$  in all measurements.

A pair of fluxgate sensors configured in a differential arrangement was used to detect the thermoelectric signals from the specimen. The primary sensor, which is closer to the specimen, measures a stronger signal than the secondary

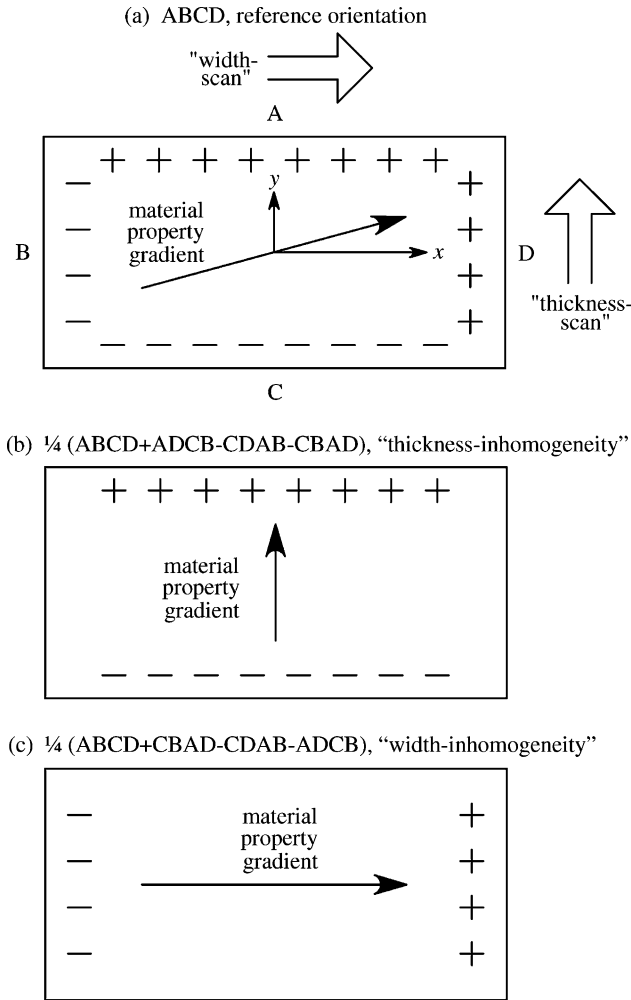


Fig. 3. A schematic drawing of (a) the two-dimensional inhomogeneity of the specimen and how addition and subtraction of different profiles can be used to eliminate either the (b) width or (c) thickness-component of the inhomogeneity.

sensor, while the two sensors exhibit essentially the same sensitivity for external sources at larger distances, which are rejected accordingly. In each case, the so called lift-off distance, i.e. the gap between the plastic case of the primary

sensor and the surface of the specimen was 2 mm. Because of the differential experimental arrangement, the magnetic field must be calculated from the analytical model at the positions of both the primary and the secondary sensors and then subtracted. However, when comparing the experimental results to the model calculations, the actual distance between the probes and the surface of the specimen should be used. The sensing element of the fluxgate is a 15 mm long ferromagnetic rod of 2 mm diameter inside a 25 mm long protective case. The specimen was scanned with both normal and tangential sensor polarization. The total distance between the effective center of the sensor and the surface of the specimen were, respectively,  $g_{pn} = 13$  mm for the primary fluxgate and  $g_{sn} = 41$  mm for the secondary fluxgate at normal polarization and  $g_{pt} = 6$  mm and  $g_{st} = 14$  mm for tangential polarization.

The magnetic signals were detected by horizontally scanning the specimen at the center of the bar in a direction normal to the heat flux. Fig. 4 showed how the normal and tangential magnetic signatures can be recorded when scanning in the ‘width-direction’ of the specimen. Since the translation table can move only horizontally, but not vertically, similar scans in the thickness-direction of the specimen were taken by rotating the specimen 90° around its axis and lying it on its thinner side. As we described above, in order to separate the ‘width’ and ‘thickness’ components of the inhomogeneity, we have to record the magnetic signature at four specimen orientations. Altogether, 16 independent signatures can be measured using eight specimen orientations and two sensor polarizations. However, all magnetic signatures were recorded with both positive and negative temperature gradient and then subtracted to separate the truly thermoelectric component from spurious contributions of external sources. Therefore, the experimental data to be presented later represents thirty-two measurements. It should be mentioned that numerous additional measures were taken to assure that the magnetic signatures were recorded with minimal distortion and these measures are described in detail in Ref. [11].

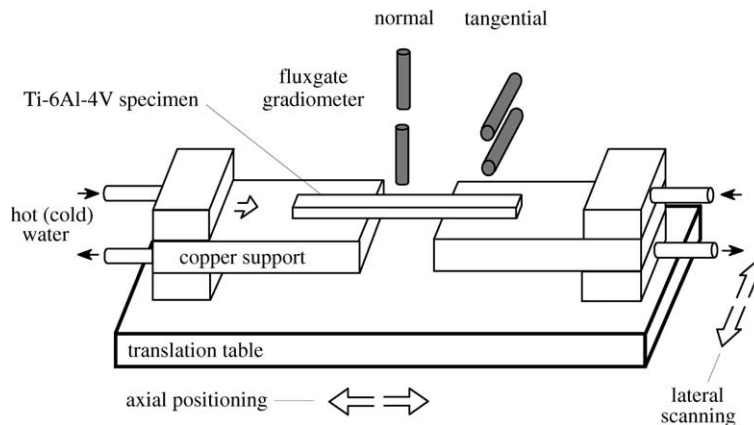


Fig. 4. A schematic diagram for the experimental arrangement.

## 4. Experimental results

### 4.1. Natural Ti–6Al–4V specimen

In order to compare the measured spatial distribution of the magnetic field due to the assumed inhomogeneity profile, we used the known geometrical dimensions of the specimen. The relevant physical parameters of Ti–6Al–4V that are needed for substitution into our analytical model are  $\sigma_0 = 5.7 \times 10^5$  A/Vm and  $S_0 = -4.9 \mu\text{V}/^\circ\text{C}$ . Two free parameters, that measure the inhomogeneity in the width  $c_x$  and thickness  $c_y$  directions, were used to find the best fit between the model predictions and the four experimentally determined signatures in each case. The average of the four best fitting values of  $c_x$  can be considered as the best estimates for the actual degree of inhomogeneity in the width-direction, while the same is true for the average of the four best fitting values of  $c_y$  and the inhomogeneity in the thickness-direction of the specimen. Though these values cannot be independently verified at this point, the fact that the four values are reasonably close to each other in both cases lends some confidence to the obtained values.

Fig. 5 shows the comparison between the experimental and theoretical thermoelectric signatures for thickness-inhomogeneity. The width-signature at normal polarization

(Fig. 5a) corresponds to  $H_y(x, y_{pn}) - H_y(x, y_{sn})$ , where  $y_{pn} = g_{pn} + t/2$  and  $y_{sn} = g_{sn} + t/2$  are the constant distances of the primary and secondary fluxgates from the  $x$ -axis at normal polarization. It was noticed that the relatively sharp peaks on the theoretical curves were always somewhat blurred on the experimental results by the finite size of the active element that reduces the spatial resolution of the measurement. Therefore, the theoretical curves were smoothed by averaging over a distance equal to the size of the fluxgate ( $\pm 7.5$  mm for tangential polarization and  $\pm 1$  mm for normal polarization) in order to simulate the reduced resolution of the experimental data. With this correction, the agreement between the shapes of the theoretical and experimental signatures is very good. The width-signature at tangential polarization (Fig. 5b) corresponds to  $H_x(x, y_{tp}) - H_x(x, y_{ts})$ , where  $y_{tp} = g_{tp} + t/2$  and  $y_{ts} = g_{ts} + t/2$  are the constant distances of the primary and secondary fluxgates from the  $x$ -axis at tangential polarization. In a similar way, Fig. 5c and d show the comparison between the experimental and theoretical thermoelectric signatures for scanning in the thickness-direction. It should be emphasized that the very good qualitative agreement between the experimental and theoretical data shown is partially due to the fact that each curve was individually best fitted by changing the thickness-inhomogeneity parameter

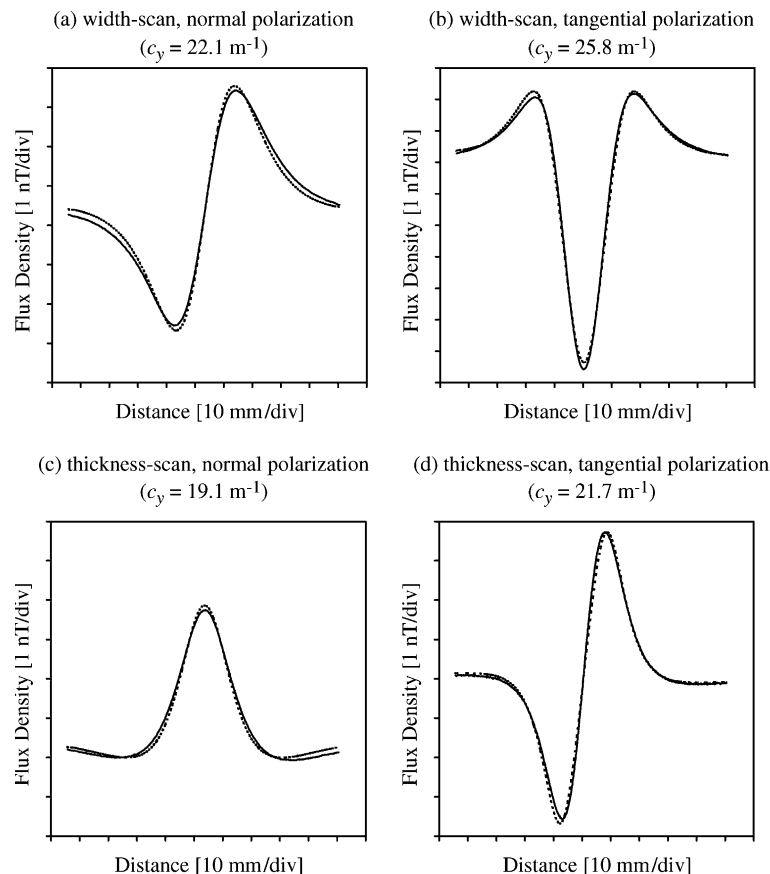


Fig. 5. Comparison between the experimental and theoretical thermoelectric signatures for thickness-inhomogeneity in the slightly inhomogeneous Ti–6Al–4V specimen (solid line, theory; dotted line, experiment).

$c_y$  (these values are listed on each figure). The average of the four  $c_y$  values was  $22.1 \text{ m}^{-1}$ , with a standard deviation of  $2.7 \text{ m}^{-1}$ , which indicates that the accuracy of the thickness-inhomogeneity assessment is  $\approx \pm 12\%$ .

Using the symmetry relationships shown in Fig. 3, the width-inhomogeneity of the specimen can be separately evaluated. Fig. 6 shows the comparison between the experimental and theoretical thermoelectric signatures caused by width-inhomogeneity of the specimen. The average value of the four  $c_x$  values was  $3.4 \text{ m}^{-1}$ , with a standard deviation of  $0.4 \text{ m}^{-1}$ , which indicates that the accuracy of the width-inhomogeneity assessment is also  $\approx \pm 12\%$ . Considering the rather crude approximations used in the theoretical calculations to account for the finite size of the sensor elements, the fact that the secondary sensor is partially shielded by the primary sensor, and the experimental errors associated with the measurement, the agreement between the experimental and theoretical thermoelectric magnetic signatures is surprisingly good.

These results verify that the observed magnetic signatures are indeed caused by a linear thermoelectric current distribution of the form  $j_z = j_{0x}x + j_{0y}y$  in the slender bar. However, the magnitude of the observed signatures raises serious doubts about the reliability of the previously described contact measurements. The  $c_x w \approx 0.043$  and  $c_y t \approx 0.14$  products represent our estimates for the total relative

variation of the thermoelectric power through the width and thickness of the slender bar, respectively. These numbers are too large to be reconciled with the independent experimental measurements by a conventional thermoelectric alloy sorter. The most probable reason for this lack of consistency is the strong anisotropy of Ti–6Al–4V [16], which preferentially crystallizes in hexagonal symmetry, and its susceptibility to measurement errors by the contact technique [4].

#### 4.2. Artificial copper/brass specimen

In order to independently verify the validity of our analytical model, we prepared an artificial specimen that exhibits a well-defined inhomogeneity that is large enough to be measured not only by the uniquely sensitive noncontacting method but also by the far less sensitive conventional contact method. For this purpose, we obtained an inhomogeneous sintered specimen made from copper and brass by powder metallurgy. This specimen was  $w = 7 \text{ mm}$  wide,  $t = 13.5 \text{ mm}$  thick, and  $\ell = 162 \text{ mm}$  long with properties varying only in the thickness ( $y$ ) direction. The composition of this sintered specimen changes from pure copper on one side to brass (80% copper, 20% zinc) on the other, which blends well at high sintering temperatures. Based on the perceivable change in color from reddish (copper) to yellowish

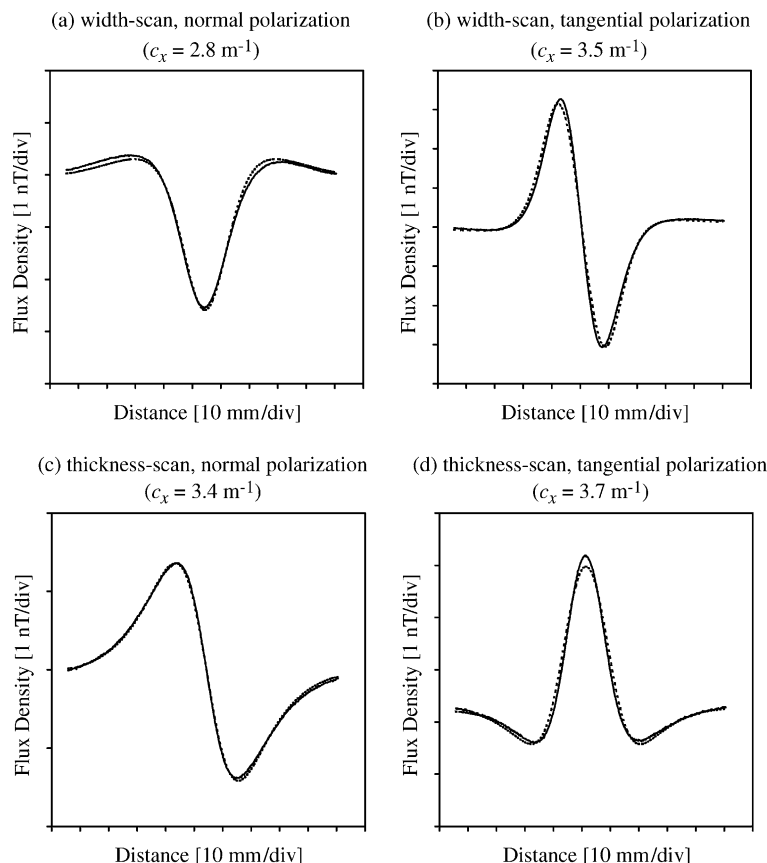


Fig. 6. Comparison between the experimental and theoretical thermoelectric signatures for width-inhomogeneity in the slightly inhomogeneous Ti–6Al–4V specimen (solid line, theory; dotted line, experiment).

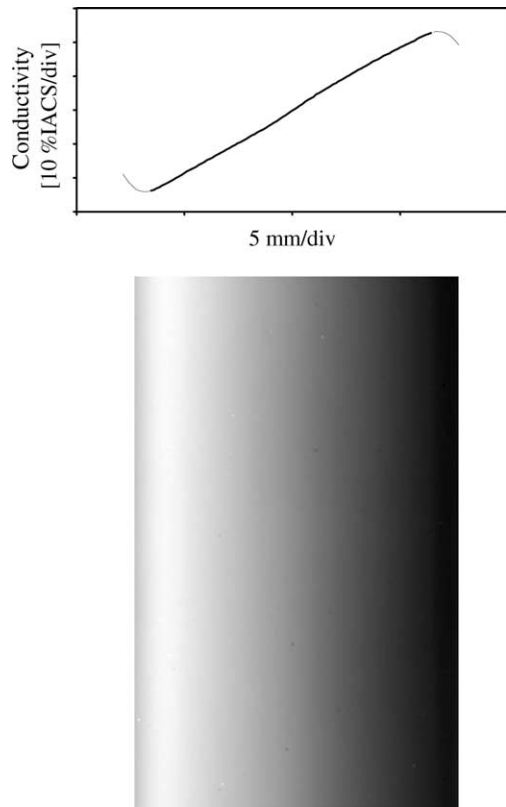


Fig. 7. Eddy current image of the conductivity variation in the artificial copper/brass reference specimen.

(brass), the transition was fairly smooth and linear. Although we had no means of actually verifying the assumed dependence of the thermoelectric power, the only parameter that is really important in our model, on position throughout the thickness of the specimen, it is reasonable to approximate this variation with a linear function changing from the thermoelectric power of pure copper to that of brass. This seems to work for the electrical conductivity, which can be mapped by scanning the side of the specimen with a small eddy current probe. Fig. 7 shows the eddy current image of the conductivity variation in this artificial copper/brass reference specimen, which was obtained by a small 1.25 mm diameter coil at 85 kHz. As in the thermoelectric measurements, this processed image was constructed by the above described averaging procedure from four raw images taken from the two sides of the specimen. The electric conductivity changed from  $\sigma_{Cu} = 79.5$  %IACS on the copper side to  $\sigma_{Br} = 29.3$  %IACS on the brass side. In our analytical calculations, we used the average of these two values, i.e.  $\sigma_0 = 54.4$  %IACS ( $3.25 \times 10^7$  A/Vm). We have also had two reference pieces made from pure copper and pure brass powder under the same conditions (sintering temperature and time) to measure their respective thermoelectric power and estimated the thermoelectric power of the inhomogeneous specimen by linear regression. The average difference in thermoelectric power between pure copper and brass was

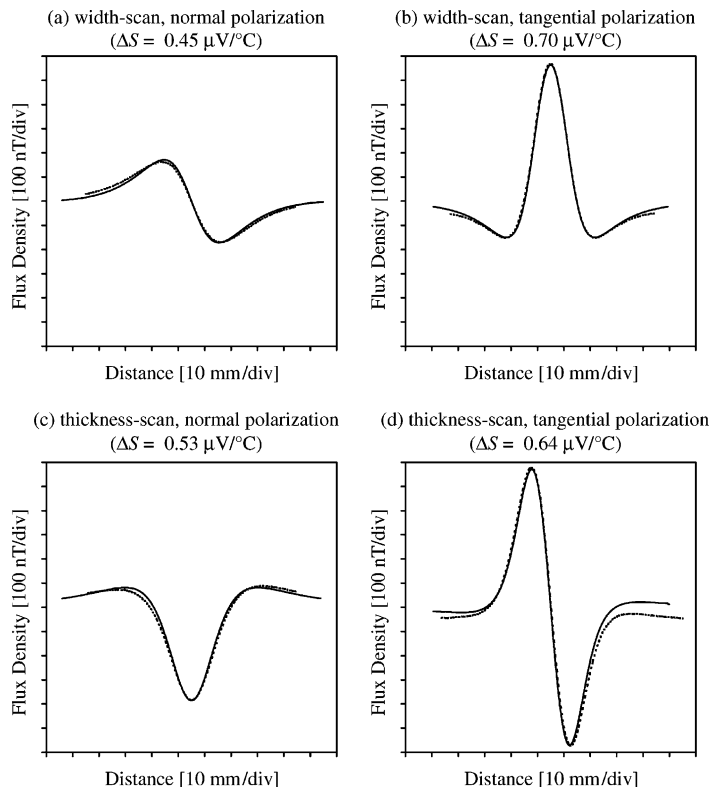


Fig. 8. Comparison between the experimental and theoretical thermoelectric signatures for thickness-inhomogeneity in the strongly inhomogeneous sintered copper/brass specimen (solid line, theory; dotted line, experiment).

found to be  $S_{Cu} - S_{Br} = \Delta S = 0.5 \mu V/^{\circ}C$ . In order to calculate the magnetic signatures predicted by our analytical model,  $\Delta S = S_{0ct}$  must be substituted into Eq. (16c).

Needless to say, this high-conductivity specimen yielded roughly two orders of magnitude stronger magnetic signals than the typical Ti–6Al–4V bar used in our previous experiment. Fig. 8 shows the comparison between the experimental and theoretical thermoelectric signatures for thickness-inhomogeneity. The temperature gradient imposed on the specimen during these measurements was  $\nabla T = 3.6 \text{ }^{\circ}C/cm$ . Again, the four signatures measured for the thickness-inhomogeneity of the specimen were individually best fitted by the predictions of our analytical model and the resulting thermoelectric contrast is listed for each case. Based on these four measurements, the average thermoelectric contrast is  $\Delta S \approx 0.57 \mu V/^{\circ}C$  with a standard deviation of  $0.08 \mu V/^{\circ}C$ , which is in very good agreement with the  $\Delta S \approx 0.5 \mu V/^{\circ}C$  value independently measured by contact means. The slight overestimation seems to be mainly caused by the data obtained at tangential polarization when the effect of the sensor size and the shielding effect of the primary sensor on the signal measured by the secondary sensor have a more significant effect on the measured overall signature. Because of these effects which would be very difficult to include in the analytical model, it appears that all the numbers obtained at tangential polarization are a little higher than those obtained at normal polarization.

The measured width-inhomogeneity (not shown) was found to be very small, roughly twenty times lower than the thickness-inhomogeneity. Of course, it should be really zero since the variation is limited to the thickness direction only, but the modest accuracy of the additions/subtractions used to separate these two effects based on their respective symmetry sets a limit on the rejection ratio. In short, our measurements on the artificial reference specimen have verified our analytical model, though at a level much higher than those encountered in real specimens. Unfortunately, this is unavoidable because the magnetic technique is orders of magnitude more sensitive than the conventional contact thermoelectric testers currently available for the limited purposes of alloys sorting.

## 5. Conclusions

This paper presented an analytical method for calculating the normal and tangential magnetic fields produced by thermoelectric currents due to the presence of weak inhomogeneity in a slender rectangular bar under axial heating and cooling. Experimental results from a Ti–6Al–4V titanium-alloy bar were shown to be in very good qualitative agreement with the predictions of the analytical model. These results clearly indicate that the observed background signatures on the four sides of the specimen can be attributed to a linear thermoelectric current distribution in the cross section of the slender bar. However, the high

magnitude of the observed signatures made it improbable that the actual source of these thermoelectric currents is simply a minor inhomogeneity of the material. Therefore, additional measurements were made on an artificial copper/brass sintered specimen that exhibited a very large thermoelectric contrast which could be measured by conventional contact thermoelectric methods. These measurements were found to be in very good quantitative agreement with our theoretical predictions and fully verified our analytical model. As for the unexpectedly high signature observed in the Ti–6Al–4V specimen, further efforts are needed to better understand the underlying physical phenomenon and to clarify the relationship between the strength of the thermoelectric signature and the very complex microstructural features of the material. However, even without positively identifying the physical source of the thermoelectric signature, we can conclude that in such specimens, the best flaw detectability can be achieved by rotating the specimen and measuring both normal and tangential magnetic signatures so that even arbitrary two-dimensional inhomogeneity could be averaged out. The results of this study can be used to optimize thermoelectric inspection procedures for flaw detection as well as to develop techniques capable of quantitatively assessing the thermoelectric inhomogeneity of metals.

## Acknowledgements

This work was supported by the US Department of Energy, Basic Energy Sciences Program under grant no. DE-FG02-00ER 45855.

## References

- [1] Henry EB, Stuart CM, Tomasulo W. Nondestructive testing handbook, vol. 9. Columbus: ASNT; 1995. p. 363–376.
- [2] Stuart CM. *J Test Eval* 1987;15:224–30.
- [3] Morgner W. *Mater Eval* 1991;9:1081–8.
- [4] Hu J, Nagy PB. *Appl Phys Lett* 1998;73:467–9.
- [5] Nagy PB, Hu J. In: Thompson DO, Chimenti DE, editors. *Review of progress in quantitative NDE*, vol. 17. New York: Plenum Press; 1998. p. 1573–80.
- [6] Hinken JH, Tavrín Y. In: Thompson DO, Chimenti DE, editors. *Review of progress in quantitative NDE*, vol. 19. Melville: AIP; 2000. p. 2085–92.
- [7] Maslov K, Kinra VK. *Mater Eval* 2001;59:1081–4.
- [8] Tavrín Y, Krivoy GS, Hinken JH, Kallmeyer JP. In: Thompson DO, Chimenti DE, editors. *Review of progress in quantitative NDE*, vol. 20. Melville: AIP; 2001. p. 1710–6.
- [9] Carreon H, Nagy PB. *Proceedings of the Seventh ASME NDE Topical Conference*, vol. 20. New York: ASME; 2001. p. 209–15.
- [10] Nagy PB, Nayfeh AH. *J Appl Phys* 2000;87:7481.
- [11] Carreon H, Nagy PB, Nayfeh AH. *J Appl Phys* 2000;88:6495.
- [12] Nayfeh AH, Carreon H, Nagy PB. *J Appl Phys* 2002;91:225.
- [13] Nayfeh AH, Faidi WI. *Eur Phys J Appl Phys* 2002;19:153.
- [14] Carreon H, Nagy PB, Blodgett MP. *Res Nondestr Eval* 2002;14:59.
- [15] Nye JF. *Physical properties of crystals, their representation by tensors and matrices*. Oxford: Clarendon Press; 1985.
- [16] Blodgett M, Nagy PB. *Appl Phys Lett* 1998;72:1045.